# We are IntechOpen, the world's leading publisher of Open Access books Built by scientists, for scientists

**4,800**
Open access books available

**122,000**
International authors and editors

**135M**
Downloads

Our authors are among the

**154**
Countries delivered to

**TOP 1%**
most cited scientists

**12.2%**
Contributors from top 500 universities

CLARIVATE ANALYTICS BOOK CITATION INDEX INDEXED

WEB OF SCIENCE™

Selection of our books indexed in the Book Citation Index in Web of Science™ Core Collection (BKCI)

## Interested in publishing with us?
## Contact book.department@intechopen.com

Numbers displayed above are based on latest data collected.
For more information visit www.intechopen.com

Chapter 3

# Finite Element Analysis of Functionally Graded Piezoelectric Spheres

A. Ghorbanpour Arani, R. Kolahchi, A. A. Mosalaei Barzoki, A. Loghman and F. Ebrahimi

Additional information is available at the end of the chapter

http://dx.doi.org/10.5772/52932

## 1. Introduction

A smart structure typically comprises of one or more active (or functional) materials. These active materials act in a unique way in which couple at least two of the following fields to provide the required functionality: mechanical, electrical, magnetic, thermal, chemical and optical. Through this coupling, these materials have the ability to change their shape, respond to external stimuli and vary their physical, geometrical and rheological properties. In modern technologies there has been an intense interest in FGPMs which are used in smart structures. It is well known that piezoelectric materials produce an electric field when deformed, and undergo deformation when subjected to an electric field. The coupling nature of piezoelectric materials has conducted wide applications in electro-mechanical and electric devices, such as electro-mechanical actuators, sensors and transducers. For example, piezoelectric actuators can be used to modify the shape of an airfoil, thereby reducing transverse vortices [1], or to maintain proper tension with overhead electrical wires on a locomotive pantograph [2].

For homogeneous piezoelectric media, problems of radially-polarized piezoelectric bodies were considered and solved analytically by Chen [3]. Sinha [4] obtained the solution of the problem of static radial deformation of a piezoelectric spherical shell and under a given voltage difference between these surfaces, coupled with a radial distribution of temperature from the inner to the outer surface. Ghorbanpour et al. [5] investigated the stress and electric potential fields in piezoelectric hollow spheres. Stress in piezoelectric hollow sphere under thermal environment was developed by Saadatfar and Rastgoo [6]. Dai and Wang [7] presented the thermo-electro-elastic transient responses in piezoelectric hollow structures. Dai and Fu [8] studied the electromagneto transient stress and perturbation of magnetic field vector in transversely isotropic piezoelectric solid spheres.

In-homogenity was considered in a number of studies. Elastic analysis of internally pressurized thick-walled spherical pressure vessels of functionally graded materials (FGMs) investigated by You et al. [9]. Analytical solution for a non-homogeneous isotropic piezoelectric hollow sphere was presented by Ding et al. [10]. Effect of material in-homogeneity on electro-thermo-mechanical behaviors of functionally graded piezoelectric rotating cylinder was considered by Ghorbanpour et al. [11]. Wang and Xu [12] studied the effect of material inhomogeneity on electromechanical behaviors of functionally graded piezoelectric spherical structures. Magnetothermoelastic problems of FGM spheres are studied by Ghorbanpour et al. [13].

Sladek et al. [14] derived Local integral equations for numerical solution of 3-D problems in linear elasticity of FGMs viewed as 2-D axisymmetric problems while the meshless local Petrov-Galerkin method was applied to transient dynamic problems in 3D axisymmetric piezoelectric solids with continuously non-homogeneous material properties subjected to mechanical and thermal loads by Sladek et al.[15]. They concluded that this method is promising for numerical analysis of multi-field problems like piezoelectric or thermoelastic problems, which cannot be solved efficiently by the conventional boundary element method.

Motivated by these ideas, new applications of piezoelectric sensors and actuators are being introduced and expanded for a number of geometric configurations. In this chapter, a hollow sphere composed of a radially polarized transversely isotropic piezoelectric material, e.g., PZT-4, which is subjected to mechanical and thermal loads, together with a potential difference induced by electrodes attached to the inner and outer surfaces of the annular sphere is considered. All mechanical, thermal and piezoelectric properties of the FGPM hollow sphere, except for the Poisson's ratio, are assumed to depend on the radius $r$ and expressed in terms of its power functions. Hence, the equation of equilibrium in the radially polarized form is reduced to a system of second–order ordinary differential equation and is solved analytically for four different sets of boundary conditions. Finally, the thermal stresses, electric potential and displacement distributions are shown for different material in-homogeneity Also, a three-dimensional finite element analysis of asymmetric closed and open spheres with different boundary conditions subjected to an internal pressure and a uniform temperature field has also been carried out using ANSYS software.

## 2. Electromechanical coupling

The subsequent characterization of electromechanical coupling covers the various classes of piezoelectric materials. Details with respect to definition and determination of the constants describing these materials have been standardized by the Institute of Electrical and Electronics Engineers [16]. Stresses $\sigma$ and strains $\varepsilon$ on the mechanical side, as well as flux density $D$ and field strength $E$ on the electrostatic side, may be arbitrarily combined as follows [17,18]

$$\begin{Bmatrix} \sigma \\ D \end{Bmatrix} = \begin{bmatrix} C^E & -e \\ e^T & \in^{\varepsilon} \end{bmatrix} \begin{Bmatrix} \varepsilon \\ E \end{Bmatrix}, \tag{1}$$

where $C^E$, $\in^{\varepsilon}$, e and $e^T$ are the fourth-order elasticity tensor, the dielectric permittivity tensor, third order tensor of piezoelectric coefficient and transpose of it, respectively.

Assuming total strain tensor to be the sum of mechanical ( $M$ ) and thermal ( $T$ ) strains [19, 20]

$$\varepsilon = \varepsilon^M + \varepsilon^T, \tag{2}$$

where

$$\varepsilon = \begin{Bmatrix} \varepsilon_{rr} \\ \varepsilon_{\theta\theta} \\ \varepsilon_{\zeta\zeta} \\ \varepsilon_{r\zeta} \\ \varepsilon_{\zeta\theta} \\ \varepsilon_{r\theta} \end{Bmatrix}, \tag{3}$$

$$\varepsilon^M = \begin{pmatrix} u_{,r} \\ \dfrac{w_{,\theta}}{r\sin\zeta} + \dfrac{\cot\zeta}{r}v + \dfrac{u}{r} \\ \dfrac{v_{,\zeta}}{r} + \dfrac{u}{r} \\ \dfrac{u_{,\zeta}}{r} + v_{,r} - \dfrac{v}{r} \\ \dfrac{v_{,\theta}}{r\sin\zeta} + \dfrac{w_{,\zeta}}{r} - \dfrac{\cot\zeta}{r}w \\ \dfrac{u_{,\theta}}{r\sin\zeta} + w_{,r} - \dfrac{w}{r} \end{pmatrix}, \qquad \varepsilon^T = \begin{pmatrix} -\alpha_r T \\ -\alpha_\theta T \\ -\alpha_\zeta T \\ 0 \\ 0 \\ 0 \end{pmatrix}, \tag{4}$$

It is also noted that the electric field tensor E can be written in terms of electric potential $\phi$ as [21]

$$\mathrm{E} = -grad\ \phi. \tag{5}$$

## 3. Formulation for electrothermoelastic FGPM spheres

A hollow FGPM sphere with an inner radius $r_i$ and outer radius $r_o$ is considered. The sphere is subjected to an internal and external pressures $P_i$ and $P_o$, an electric potential $\varphi$ and a distributed temperature field $T(r)$ (Fig. 1). It is assumed that, only the radial displacement $U_r$ is nonzero and electric potential is the functions of radial coordinate $r$, Thus

$$U_r = u(r),\ U_\zeta = U_\theta = 0,\ \phi = \phi(r). \tag{6}$$

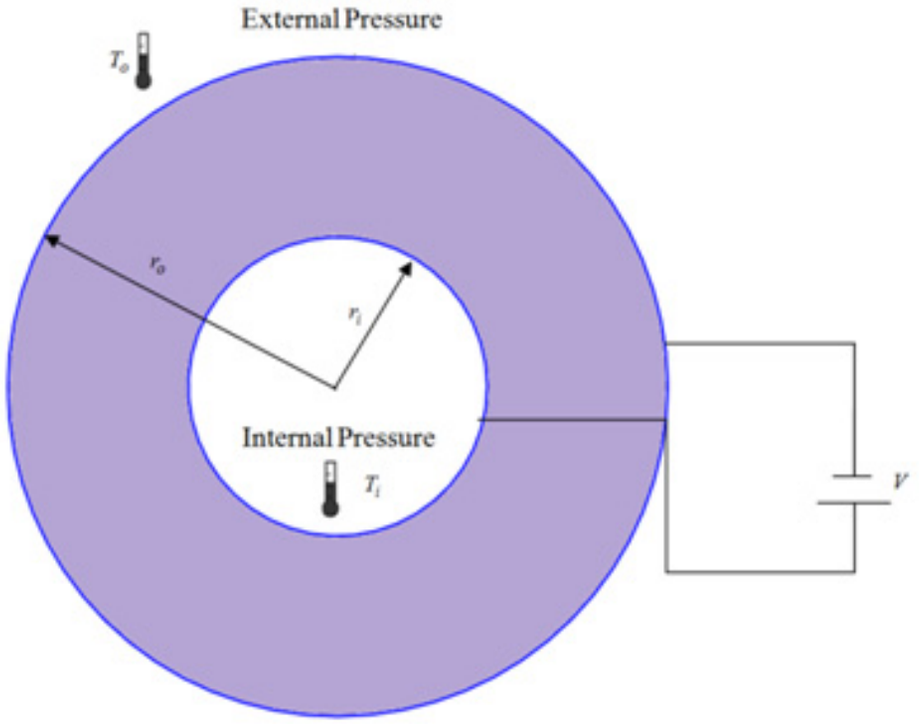


**Figure 1.** Hollow FGPM sphere subject to uniform temperature field, uniform internal pressure, uniform external pressure and applied voltage V.

The equilibrium equation of the FGPM sphere in the absence of body force and the Maxwell's equation for free electric charge density are [18, 22]

$$\sigma_{rr,r} + \frac{2(\sigma_{rr} - \sigma_{\theta\theta})}{r} = 0, \tag{7}$$

$$D_{rr,r} + \frac{2}{r} D_{rr} = 0, \tag{8}$$

where $\sigma_{ii}\left(i = r, \theta\right)$ is the stress tensor and $D_{rr}$ is the radial electric displacement.

Also, the radial and circumferential strain and the relation between electric field and electric potential are reduced to

$$\varepsilon_{rr} = u_{,r}, \tag{9}$$

$$\varepsilon_{\theta\theta} = \varepsilon_{\zeta\zeta} = \frac{u}{r}, \tag{10}$$

$$E_{rr} = -\phi_{,r}. \tag{11}$$

The constitutive relations of spherically radially polarized piezoelectric media and the component of radial electric displacement vector also can be written as [23, 24]

$$\begin{Bmatrix}\sigma_{rr}\\ \sigma_{\theta\theta}\\ \sigma_{\zeta\zeta}\\ D_{rr}\end{Bmatrix}=\begin{bmatrix}C_{11} & C_{12} & C_{13} & e_{11}\\ C_{21} & C_{22} & C_{23} & e_{12}\\ C_{31} & C_{32} & C_{33} & e_{13}\\ e_{11} & e_{12} & e_{13} & -\in_{11}\end{bmatrix}\begin{Bmatrix}\varepsilon_{rr}-\alpha_r T(r)\\ \varepsilon_{\theta\theta}-\alpha_\theta T(r)\\ \varepsilon_{\zeta\zeta}-\alpha_\zeta T(r)\\ E_{rr}\end{Bmatrix} \tag{12}$$

For transversely isotropic properties, when the concerned axis of rotation is oriented in the radial direction, the elasticity and piezoelectric coefficient tensors are summarized to [25]

$$C_{12}=C_{13}=C_{21},\quad C_{22}=C_{33},\quad C_{32}=C_{23},\qquad e_{12}=e_{13}. \tag{13}$$

It is appropriate to introduce the following dimensionless quantities as

$$\begin{aligned}&\sigma_i=\frac{\sigma_{ii}}{C_{22}}\left(i=r,\theta\right),\ c_i=\frac{C_{1i}}{C_{22}}\left(i=1,2,3\right),\quad E_i=\frac{e_{1i}}{E_0}\left(i=1,2,3\right),\qquad E_0=\sqrt{C_{22}\in_{11}},\\ &U=\frac{u_r}{r_i},\quad \xi=\frac{r}{r_i},\quad \eta=\frac{r_o}{r_i},\quad \beta=\frac{\beta_1}{E_0},\quad \Phi=\frac{\phi}{\phi_0},\quad \phi_0=r_i\sqrt{\frac{C_{22}}{\in_{11}}},\qquad D_r=\frac{D_{rr}}{E_0}.\end{aligned} \tag{14}$$

Using the above dimensionless variables, Eqs. (7) and (8) can be expressed as

$$\sigma_{r,\xi}+\frac{2\left(\sigma_r-\sigma_\theta\right)}{\xi}=0, \tag{15}$$

$$D_{r,\xi}+\frac{2D_r}{\xi}=0. \tag{16}$$

Before substituting the component of the electric field in Maxwell's equation, appropriate power functions for all properties are assumed as [26]

$$\Gamma_r=\Gamma_0\left(\xi\right)^\gamma, \tag{17}$$

in which $\Gamma_r$ represents the general properties of the sphere such as the elastic, piezoelectric, dielectric coefficients and thermal conductivity, and $\Gamma_0$ corresponds to the value of the coefficients at the outer surface. Substituting Eqs. (14) and (17) into Eq. (12), yields

$$\begin{Bmatrix}\sigma_r\\ \sigma_\theta\\ \sigma_\zeta\\ D_r\end{Bmatrix}=\xi^\gamma\left(\begin{bmatrix}C_1 & C_2 & C_2 & E_1\\ C_2 & 1 & C_3 & E_2\\ C_2 & C_3 & 1 & E_2\\ E_1 & E_2 & E_2 & -1\end{bmatrix}\begin{Bmatrix}U_{,\xi}-\xi^\gamma\alpha_r T(\xi)\\ \frac{U}{\xi}-\xi^\gamma\alpha_\theta T(\xi)\\ \frac{U}{\xi}-\xi^\gamma\alpha_\theta T(\xi)\\ \Phi_{,\xi}\end{Bmatrix}\right) \tag{18}$$

## 4. Electrothermoelastic analysis of FGPM spheres

The solution of Eq. (16) is

$$D_r = \frac{A_1}{\xi^2}, \tag{19}$$

where $A_1$ is a constant. Substituting Eq. (19) into Eq. (18), we obtain

$$\begin{Bmatrix}\sigma_r \\ \sigma_\theta\end{Bmatrix} = \xi^{\gamma}\left(\left(\begin{bmatrix}C_1 & C_2 & C_2 \\ C_2 & 1 & C_3\end{bmatrix}+\begin{bmatrix}E_1^2 & E_1E_2 & E_1E_2 \\ E_1E_2 & E_2^2 & E_2^2\end{bmatrix}\right)\left(\begin{Bmatrix}U_{,\xi}-\xi^{\gamma}\alpha_r T(\xi) \\ \frac{U}{\xi}-\xi^{\gamma}\alpha_\theta T(\xi) \\ \frac{U}{\xi}-\xi^{\gamma}\alpha_\theta T(\xi)\end{Bmatrix}\right)-\begin{bmatrix}E_1 \\ E_2\end{bmatrix}\left(A_1\xi^{-\gamma-2}\right)\right) \tag{20}$$

In this study a distributed temperature field due to steady-state heat conduction has been considered. Using Eq. (17) for the thermal conductivity property, the heat conduction equation without any heat source is written in spherical coordinate as [22, 27]

$$\frac{1}{\xi^2}\left(K_0\,\xi^{\gamma+2}\,T(\xi)_{,\xi}\right)_{,\xi} = 0, \tag{21}$$

$$\begin{aligned} &at\ \xi = 1 \qquad T(\xi) = T_a, \\ &at\ \xi = \eta \qquad T(\xi)_{,\xi} + hT(\xi) = 0, \end{aligned} \tag{22}$$

where $h$ is the ratio of the convective heat-transfer coefficient and $K_0$ is the nominal heat conductivity coefficient. Integrating Eq. (21) twice yields

$$T(\xi) = -\frac{B_1}{\gamma+1}\xi^{-\gamma-1} + B_2, \tag{23}$$

Constants $B_1$ and $B_2$ are obtained using thermal boundary conditions which shown in Eq. (22).

Finally, substituting Eq. (20) and (24) into Eq. (15) yields the following non-homogeneous Cauchy differential equation

$$\xi^2\frac{\partial^2 U}{\partial\,\xi^2} + D_1\xi\frac{\partial U}{\partial\xi} + D_2U = D_4B_1 + D_5B_2\xi^{(1+\gamma)} + D_3A_1\xi^{-(1+\gamma)} \tag{24}$$

where $D_i\left(i = 1,...8\right)$ are defined in Appendix A.

The exact solution for Eq. (24) is written as follows

$$u_g = \underbrace{K_1\exp(q_1\xi)}_{u_{g1}} + \underbrace{K_2\exp(q_2\xi)}_{u_{g2}}, \tag{25}$$

$$q_1, q_2 = \frac{(1-D_1) \pm \sqrt{\left(D_1-1\right)^2 - 4D_2}}{2}. \tag{26}$$

The particular solution of the differential Eq. (24) may be obtained as

$$u_p = \xi^{q_1} u_1 + \xi^{q_2} u_2, \tag{27}$$

where

$$u_1 = -\int \frac{\xi^{q_2} R(\xi)}{W(q_1, q_2)}, \qquad u_2 = \int \frac{\xi^{q_1} R(\xi)}{W(q_1, q_2)}, \tag{28}$$

in which $R(\xi)$ is the expression on the right hand side of Eq. (24) and $W(\xi)$ is defined as

$$W(q_1, q_2) = \begin{vmatrix} u_{g1} & u_{g2} \\ (u_{g1})' & (u_{g2})' \end{vmatrix}. \tag{29}$$

Combining Eqs. (25)-(29) one can obtain the particular solution as

$$u_p = \frac{D_3 \xi^{1-\gamma}}{(q_2 + \gamma - 1)(q_1 + \gamma - 1)} A_1 + \frac{D_5 \xi^{3+\gamma}}{(3 - q_2 + \gamma)(3 - q_1 + \gamma)} B_2 + \frac{D_4 \xi^3}{(q_2 - 3)(q_1 - 3)} B_1. \tag{30}$$

The complete solution for $U^m$ in terms of the non-dimensional radial coordinate is written as

$$U = u_g + u_p, \tag{31}$$

where $K_1$, $K_2$ and $A_1$ are unknown constants. Substituting the displacement from Eq. (31) into Eq. (20) the radial and circumferential stresses are obtained as

$$\begin{aligned} \sigma_r(\xi) = & \left( \left( 2C_2 + C_1 q_1 + 2E_1 E_2 + E_1^2 q_1 \right) \xi^{q_1 - 1 + \gamma} \right) K_1 + \left( \left( 2C_2 + C_1 q_2 + 2E_1 E_2 + E_1^2 q_2 \right) \xi^{q_2 - 1 + \gamma} \right) K_2 \\ & + \left( \frac{\left( 2C_2 + 2E_1 E_2 + (3+\gamma)(E_1^2 + C_1) \right) D_4 \xi^2}{(q_2 - 3)(q_1 - 3)} + \frac{\left( 2(C_2 + E_1 E_2)\alpha_\theta + (E_1^2 + C_1)\alpha_r \right) \xi^{\gamma - 1}}{\gamma + 1} \right) B_1 \\ & + \left( \frac{\left( 2C_2 + 2E_1 E_2 + (3+\gamma)(E_1^2 + C_1) \right) D_5 \xi^{2+2\gamma}}{(3 - q_2 + \gamma)(3 - q_1 + \gamma)} - \left( 2(C_2 + E_1 E_2)\alpha_\theta + (E_1^2 + C_1)\alpha_r \right) \xi^{2\gamma} \right) B_2 \\ & + \left( \frac{\left( 2C_2 + 2E_1 E_2 + (1-\gamma)(E_1^2 + C_1) \right) D_3}{(q_2 + \gamma - 1)(q_1 + \gamma - 1)} - 2\left( E_1 \right) \xi^{-2} \right) A_1 \end{aligned} \tag{32}$$

$$\begin{aligned}\sigma_\theta(\xi) &= \left(\left(C_3 + C_2 q_1 + E_1 E_2 q_1 + 2E_2^2 + 1\right)\xi^{q_1 - 1+\gamma}\right)K_1 + \left(\left(C_3 + 2E_2^2 + E_1 E_2 q_2 + C_2 q_2 + 1\right)\xi^{q_2 - 1+\gamma}\right)K_2 \\ &+ \left(\frac{\left(C_3 + 3C_2 + 2E_2^2 + 3E_1 E_2 + 1\right)D_4 \xi^{2+\gamma}}{(q_2 - 3)(q_1 - 3)} + \frac{\left((C_3 + 2E_2^2 + 1)\alpha_\theta + (C_2 + E_1 E_2)\alpha_r\right)\xi^{\gamma-1}}{\gamma + 1}\right)B_1 \\ &+ \left(\frac{\left(C_3 + 2E_2^2 + 1 + (3+\gamma)(E_1 E_2 + C_2)\right)D_5 \xi^{2+2\gamma}}{(3 - q_2^m + \gamma)(3 - q_1^m + \gamma)} - \left((1 + C_3 + 2E_2^2)\alpha_\theta + (C_2 + E_1 E_2)\alpha_r\right)\xi^{2\gamma}\right)B_2 \\ &+ \left(\frac{\left(C_3 + 2E_1 E_2 + 2E_2^2 + 1 + (1-\gamma)(E_1 E_2 + C_2)\right)D_3}{(q_2 + \gamma - 1)(q_1 + \gamma - 1)} - E_2 \xi^{-2}\right)A_1\end{aligned} \tag{33}$$

Substituting $U$ from above into the last term of Eq. (18), ($\Phi_{,\xi}$) and combining with Eq. (19) and performing the integrating, electric potential is obtained as

$$\begin{aligned}\Phi(\xi) &= \left(\left(\frac{2E_2}{q_1} + E_1\right)\xi^{q_1}\right)K_1 + \left(\left(\frac{2E_2}{q_2} + E_1\right)\xi^{q_2}\right)K_2 \\ &+ \left(\frac{\left(\gamma E_1 - E_1 - 2E_2\right)D_3 \xi^{1-\gamma}}{(q_2 + \gamma - 1)(q_1 + \gamma - 1)(1-\gamma)} + \frac{\xi^{-\gamma-1}}{(1+\gamma)}\right)A_1 \\ &+ \left(\frac{(E_1 + 2/3\, E_2)D_4 \xi^3}{(q_2 - 3)(q_1 - 3)} + \frac{(2E_2\alpha_\theta + E_1\alpha_r)\ln(\xi)}{\gamma + 1}\right)B_1 \\ &+ \left(\frac{\left(3E_1 + \gamma E_1 + 2E_2\right)D_5 \xi^{\gamma+3}}{(q_2 + \gamma - 1)(q_1 + \gamma - 1)(3+\gamma)} - \frac{(2E_2\alpha_\theta + E_1\alpha_r)\xi^{\gamma+1}}{\gamma + 1}\right)B_2 + A_2,\end{aligned} \tag{34}$$

where $\sigma_r$, $\sigma_\theta$ and $\Phi$ are radial stress, hoop stress and electric potential, respectively. Two sets of mechanical and electrical loading boundary conditions are considered in this investigation which in normalized form are written as

$$\text{case 1}: \sigma_r(1) = -1, \ \sigma_r(\eta) = 0, \ \ \Phi(1) = 0, \ \ \Phi(\eta) = 0 \tag{35}$$

$$\text{case 2}: \sigma_r(1) = 0, \ \ \sigma_r(\eta) = 0, \ \ \Phi(1) = 1, \ \ \Phi(\eta) = 0 \tag{36}$$

In case 1, the FGPM hollow sphere is subjected to an internal uniform pressure without any imposed electric potential and external pressure. However in this case the induced electric potential existed across the thickness. In this case, the sphere acts as an sensor. In the second case, an electrical potential difference is applied between the inner and outer surfaces of the sphere without any internal and external pressures. In this case, the sphere acts as an actuator.

For the above mentioned cases 1, and 2 the system of linear algebraic equations for the constants $K_1$, $K_2$, $A_1$ and $A_2$ of the Eqs. (32), (33) and (34) can be written in the following from

$$\begin{bmatrix} K_1 \\ K_2 \\ A_1 \\ A_2 \end{bmatrix} = inv\left(\begin{bmatrix} m_{11} & m_{12} & m_{13} & m_{14} \\ m_{21} & m_{22} & m_{23} & m_{24} \\ m_{31} & m_{32} & m_{33} & m_{34} \\ m_{41} & m_{42} & m_{43} & m_{44} \end{bmatrix}\right) \times \begin{bmatrix} b_1 \\ b_2 \\ b_3 \\ b_4 \end{bmatrix}, \tag{37}$$

where the $m_{ij}$ and $b_i$ $(i, j = 1,...4)$ are defined in Appendix B

## 5. Numerical results and discussion

### 5.1. Analytical solution

The numerical results are showing the variation of stresses, electric potential and displacement across the thickness of the FGPM sphere for different material inhomogenity parameter $\gamma$ . Presented results are for the two cases of different boundary conditions with aspect ratio $\eta = 1.3$ . The plots in these figures correspond to $T_i = 323K$ and $T_o = 298K$ . The piezoelectric material PZT-4 has been selected because of its technical applications. Mechanical and electrical properties of piezoelectric material, PZT-4 are tabulated in Table 1[28].

| ***Property*** | $C_{11}$ | $C_{12}$ | $C_{22}$ | $C_{23}$ | $e_{11}$ | $e_{12}$ | $e_{11}$ | | $\alpha_{r0}$ | $\rho$ |
|---|---|---|---|---|---|---|---|---|---|---|
| ***PZT-4*** | 115 *Gpa* | 74.3 *Gpa* | 139 *Gpa* | 77.8 *Gpa* | 15.1 $C/m^2$ | -5.2 $C/m^2$ | 3.87e-9 $F/m$ | 2 e - 5 $1/K$ | 2 e -6 $1/K$ | *7500* $kg/m^3$ |

**Table 1.** Mechanical, electrical and thermal properties for PZT-4

#### *5.1.1. Case 1*

Results of the first case are illustrated in Figs. 2 to 5. Radial stresses for different material in-homogeneity parameters $\gamma$ are shown in Fig. 2. Radial stresses satisfy the mechanical boundary conditions at the inner and outer surfaces of the FGPM sphere. The maximum absolute values of radial stresses belong to a material identified by in-homogeneity parameter $\gamma = 1.5$ the minimum absolute values of which belong to $\gamma = -1.5$ . In this case there is no imposed electric potential however, the induced electric potentials for different material in-homogeneity parameters $\gamma$ are shown in Fig. 3. Electric potentials satisfy the electrical boundary conditions at the inner and outer surfaces of the FGPM sphere. It is also obvious that higher induced electric potentials belong to higher absolute values of compressive radial stresses. In this case circumferential stresses shown in Fig. 4 are highly tensile throughout thickness and except for the material $\gamma = 1.5$ their maximum values located at the inner and their minimum values located at the outer surfaces of the sphere. Displacements are illustrated in Fig. 5 for all material properties. Displacements are positive throughout the thickness and they smoothly decrease from their maximum value at the

inner surface to their minimum value at the outer surface of the FGPM sphere. Maximum values of displacements belong to $\gamma = -1.5$ and minimum values belong to $\gamma = 1.5$

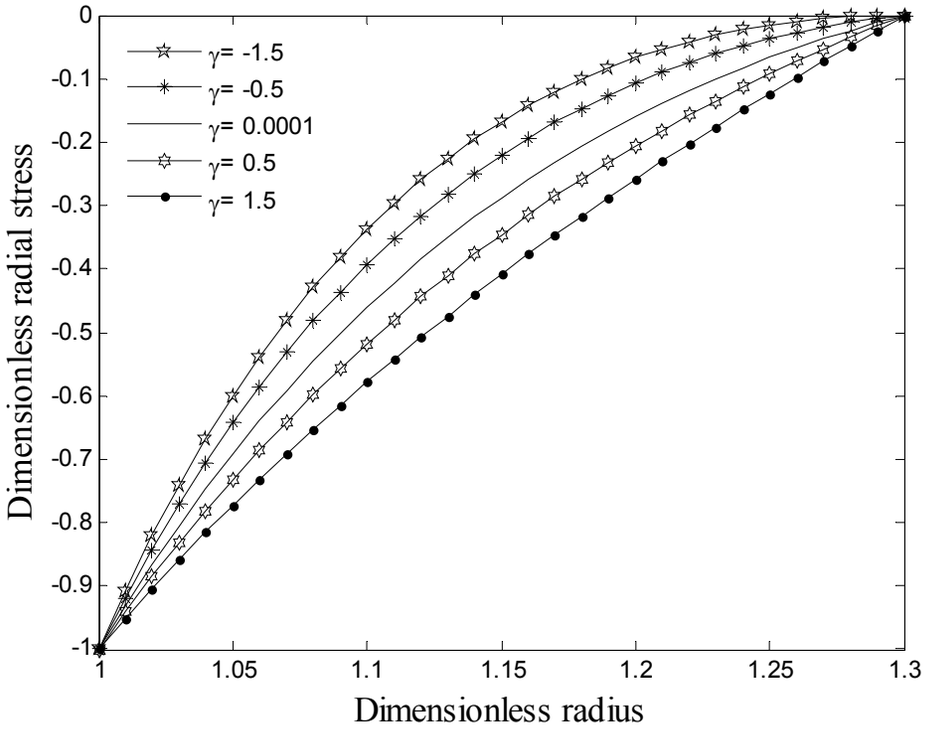


**Figure 2.** Case 1: Distributions of the radial stress for different values of $\gamma$.

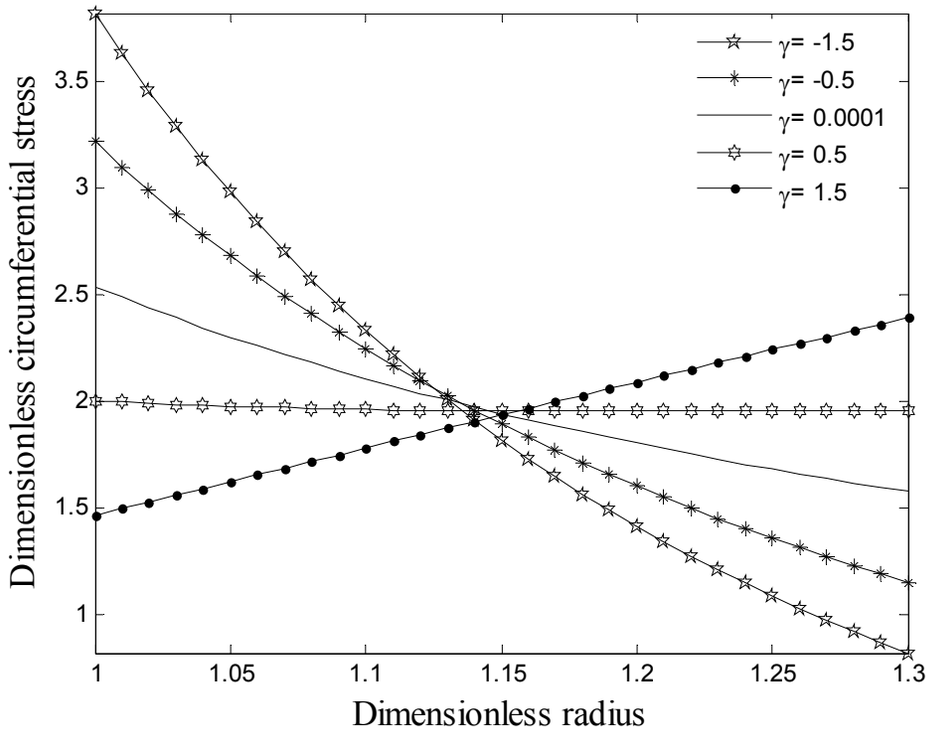


**Figure 3.** Case 1: Distributions of the circumferential stress for different values of $\gamma$.

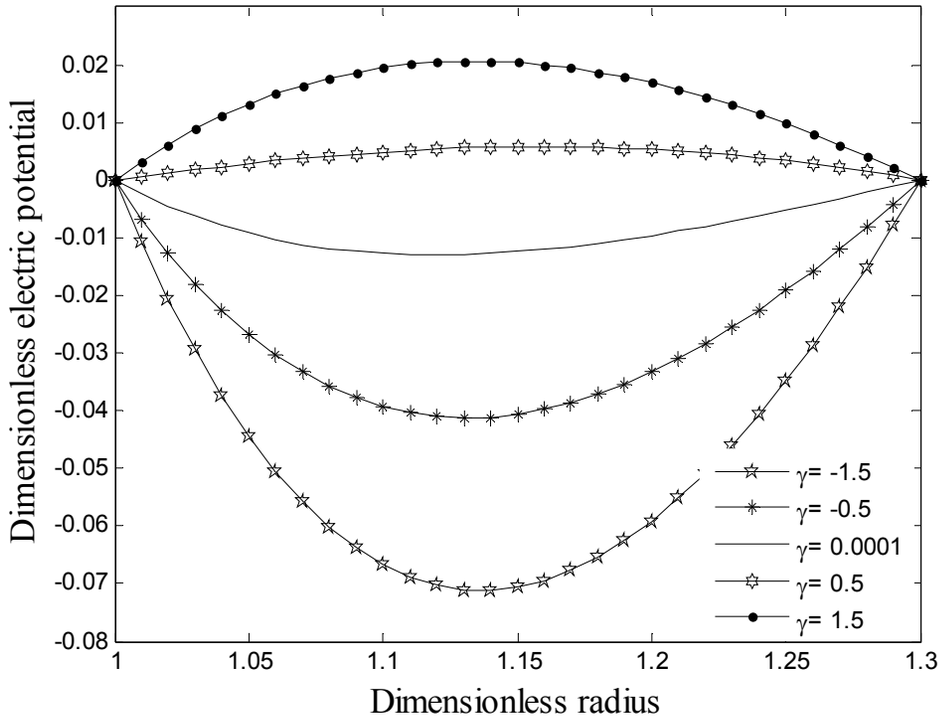


**Figure 4.** Case 1: Distributions of the electric potential for different values of $\gamma$.

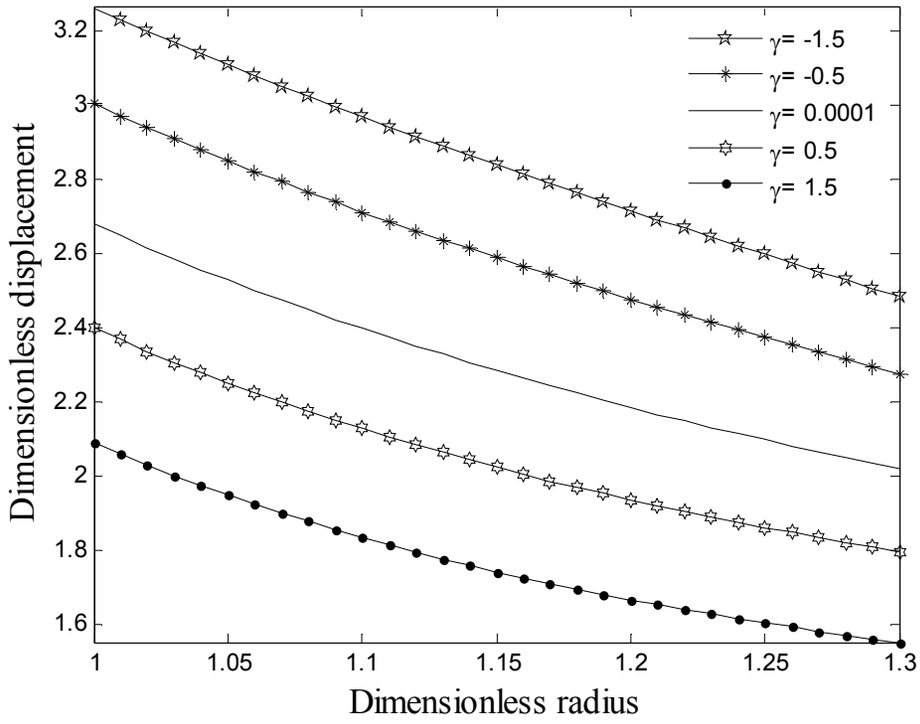


**Figure 5.** Case 1: Distributions of the radial displacement for different values of $\gamma$.

### *5.1.2. Case 2*

Results of this case are illustrated in Figs. 6 to 9. In this case the imposed electric potential satisfies the electrical boundary conditions at the inner and outer surfaces of the sphere. The maximum electric potentials belong to $\gamma = -1.5$ the minimum values of which belong to $\gamma = 1.5$ . In this case there is no applied pressure at the inner and outer surfaces of the sphere however the induced compressive radial stresses satisfy the free mechanical boundary conditions. The maximum absolute values of the induced compressive radial stresses belong to the same maximum value of electric potential. Circumferential induced stresses are compressive throughout thickness for different material in-homogeneity parameters $\gamma$ . However, for negative parameters $\gamma$ the minimum values of circumferential stresses located at the inner surface while for positive parameters $\gamma$ their minimum values located at the outer surface of the FGPM sphere. The induced displacement is negative across the thickness for all material parameters. Their minimum values located at the inner and their maximum values located at the outer surfaces of the FGPM sphere. It is interesting to compare the induced radial and circumferential stresses in this case with the residual stresses locked in the sphere during the autofrettage process of spheres made of uniform material. One might conclude that by easily imposing an electric potential there is no need to autofrettage these vessels.

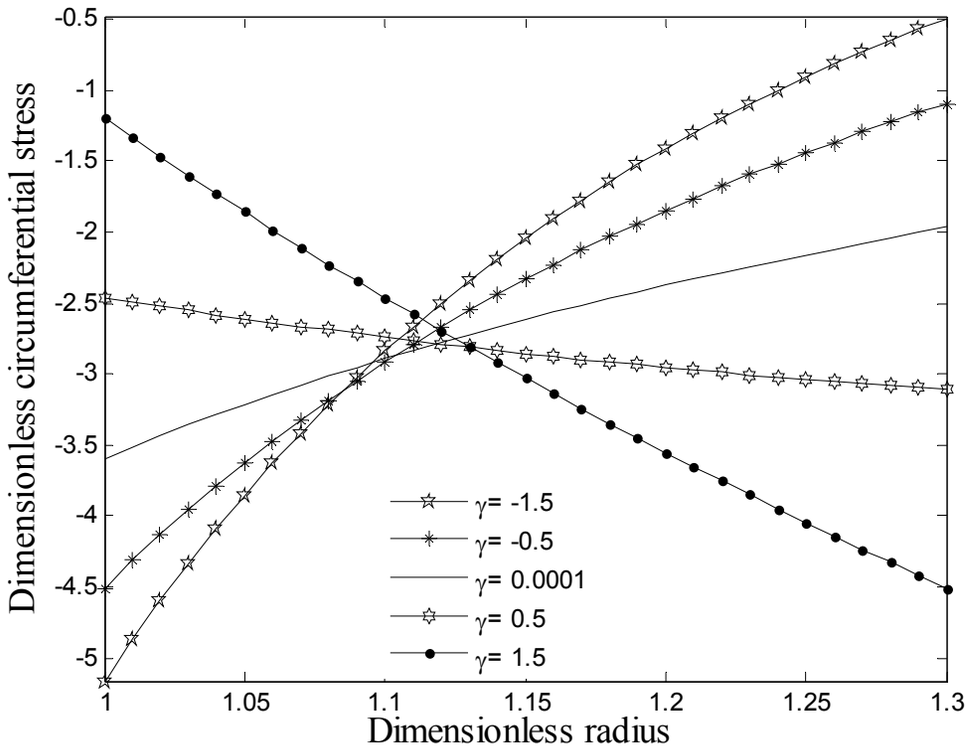


**Figure 6.** Case 2: Distributions of the radial stress for different values of $\gamma$.

## 5.2. Validation

The results of this investigation are validated with the recently published paper by Wang and Xu [12] which is shown in Figs. 10 and 11. There are a very good agreement among the

results and the only small differences are due to thermal stresses which are not considered by Wang and Xu .

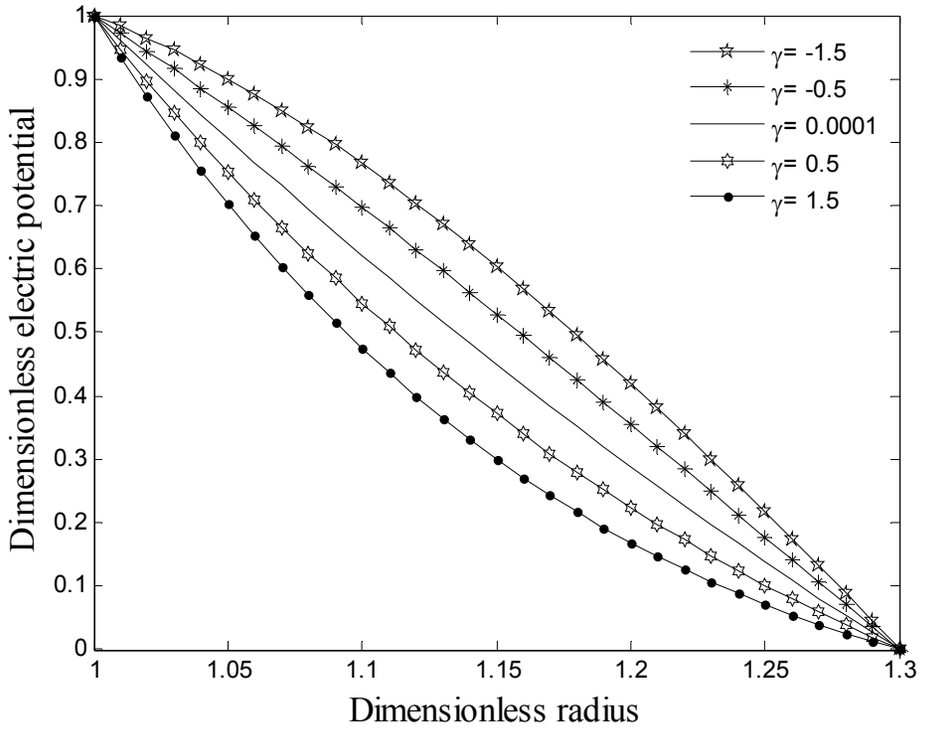


**Figure 7.** Case 2: Distributions of the circumferential stress for different values of $\gamma$.

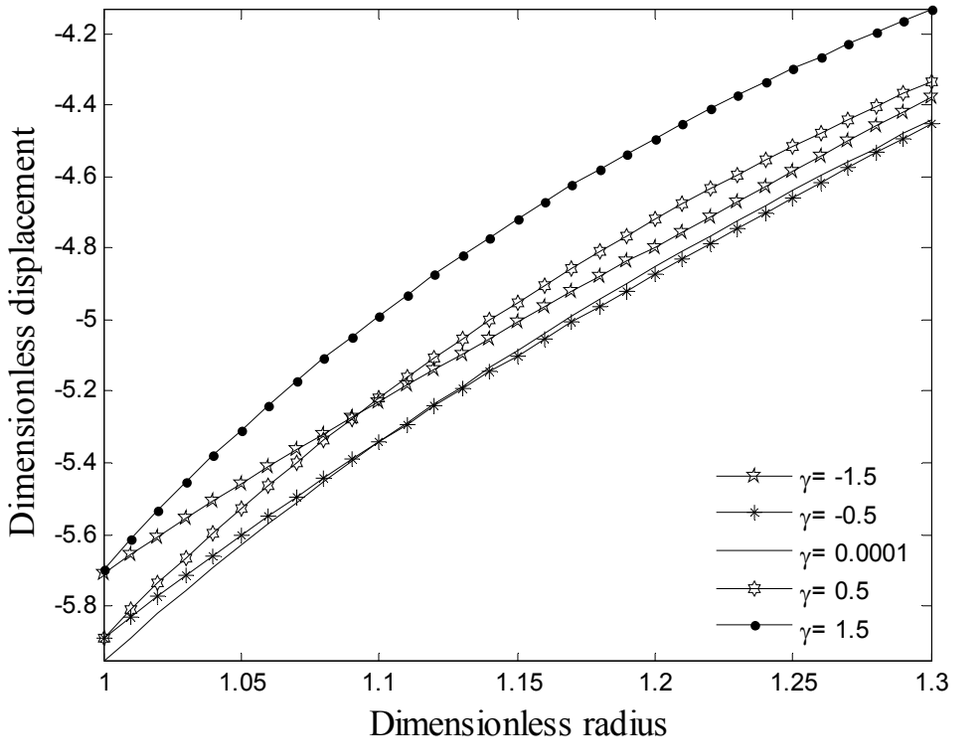


**Figure 8.** Case 2: Distributions of the electric potential for different values of $\gamma$.

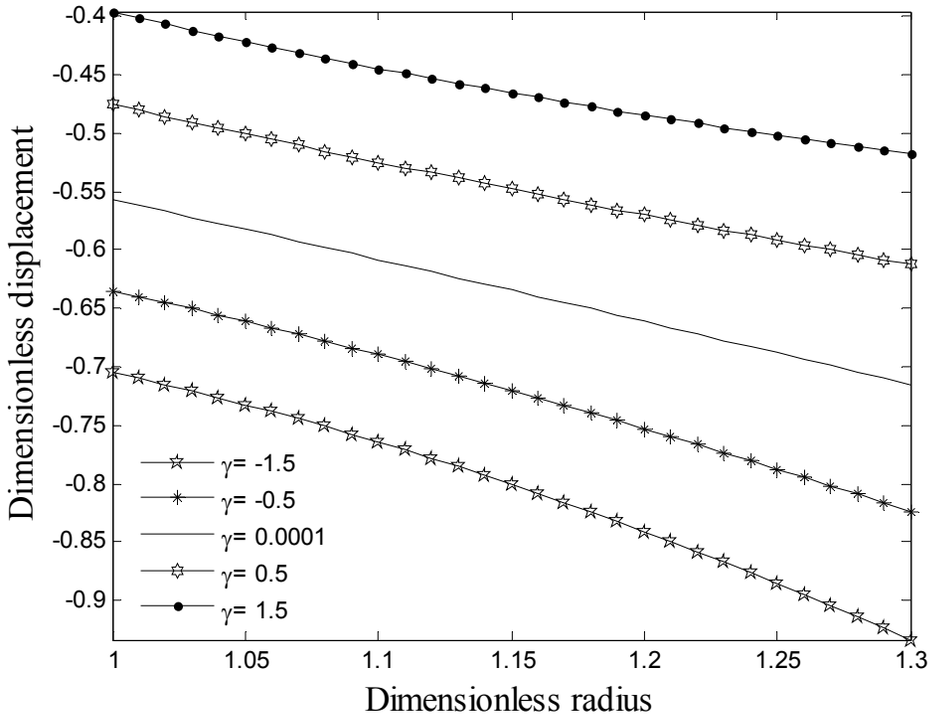


**Figure 9.** Case 2: Distributions of the radial displacement for different values of $\gamma$.

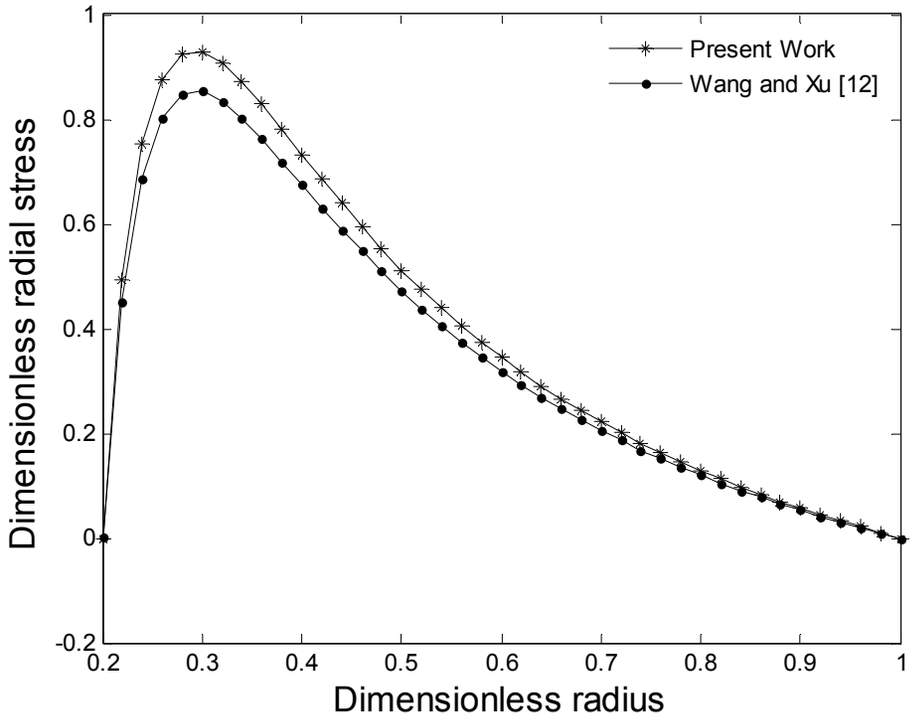


**Figure 10.** Case 2: Comparison of the radial stress distributions with Ref. [12] for homogeneous piezoelectric hollow sphere.

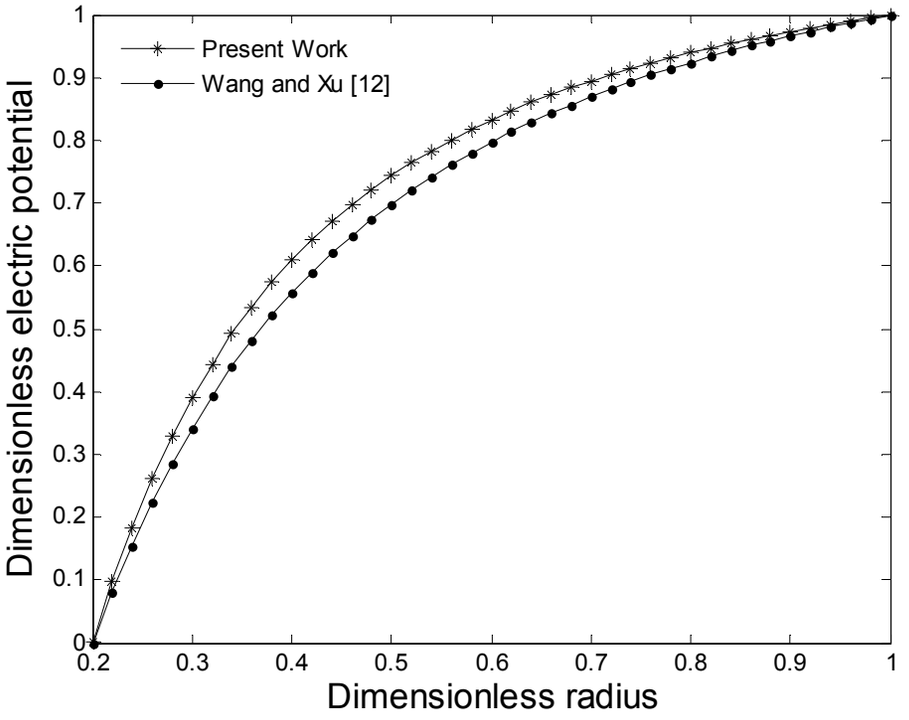


**Figure 11.** Case 2: Comparison of the electric potential distributions with Ref. [12] for homogeneous piezoelectric hollow sphere.

## 5.3. Finite element solution

In order to develop the one-dimensional solution to a three-dimensional approach finite element analysis of a sphere subjected to an internal pressure and a uniform temperature field has been carried out using ANSYS finite element software. A three-dimensional element identified by solid 191 is selected because it is an appropriate element for the FGPM structures. Sphere has been divide into eight layers by a controlled mesh system along radius and the mechanical, electrical and thermal properties are functionally defined according to power law Eq. (17) for $\gamma = 1.5$ . A controlled mesh in which very fine elements are located at the supports where stress concentration existed is employed in this method. However farther from the supports a coarser mesh is dominated. In this work, two cases for sphere are considered as follows:

### *5.3.1. Three- dimensional sphere*

In this case, consider a sphere with two asymmetric simply supported boundary conditions on the outer surface of the sphere as shown in Fig. 12. For this boundary condition dimensionless effective stresses versus normalized radius at two cross sections (i.e. A-A and B-B) are depicted in Fig. 13. Section A-A is selected to pass through supported point on the outer surface of the sphere and section B-B is an arbitrary section as shown in Fig. 12. It can be seen from this figure that the maximum effective stress for the above mentioned sections occur at the inner surface of the sphere and the effective stresses are decreasing with increasing radius for $\eta = 1.3$ . Total dimensionless displacement versus dimensionless radius

for $\eta = 1.3$ at two cross sections of A-A and B-B are demonstrated in Fig. 14. As can be seen from this figure the maximum displacement occur at the inner surface of the sphere and displacement value is decreasing with increasing dimensionless radius so that for section A-A, the zero value of displacement at the outer surface satisfies the boundary condition at this point.

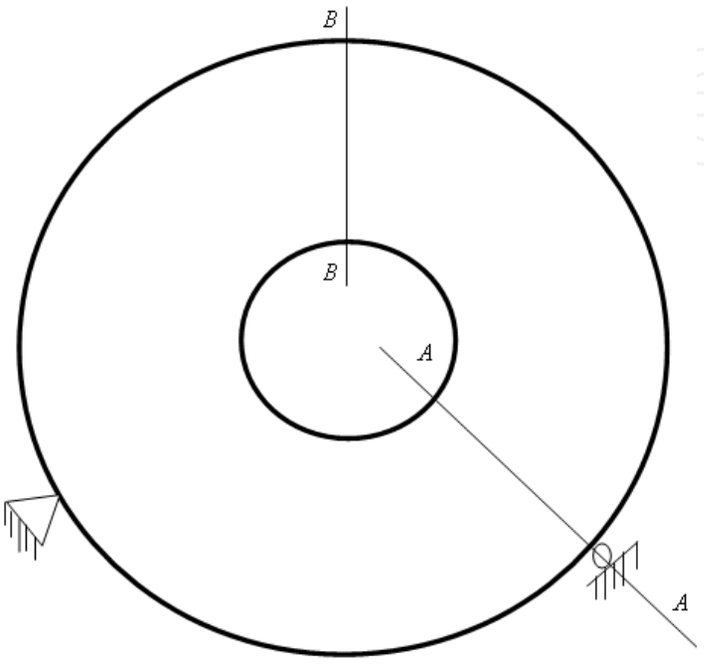


**Figure 12.** A schematic of asymmetric thick-walled sphere with simply-simply supported.

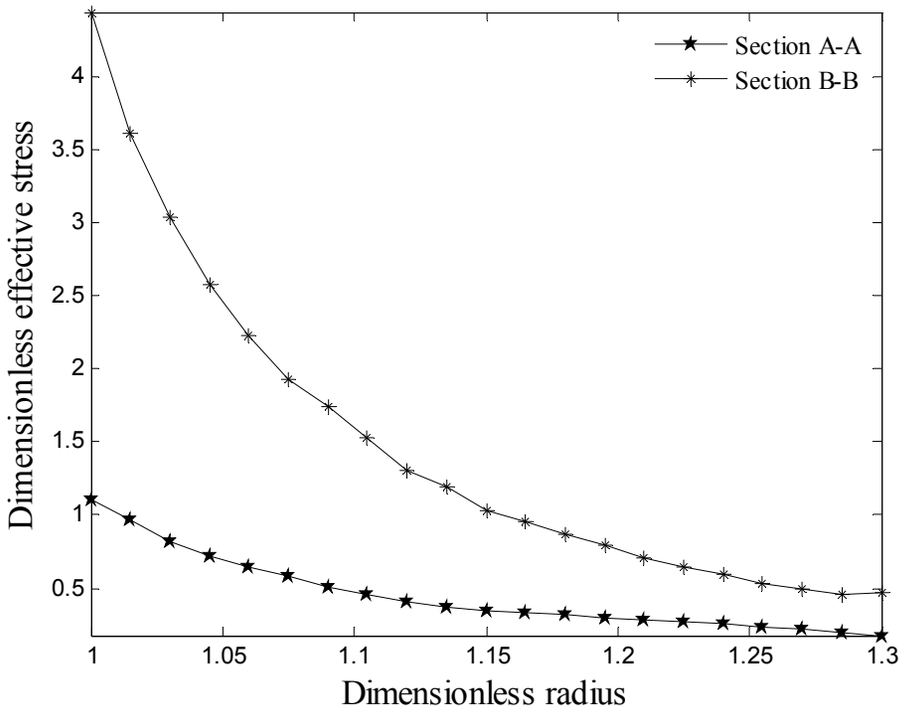


**Figure 13.** Effective stress distribution along the radius of asymmetric closed sphere.

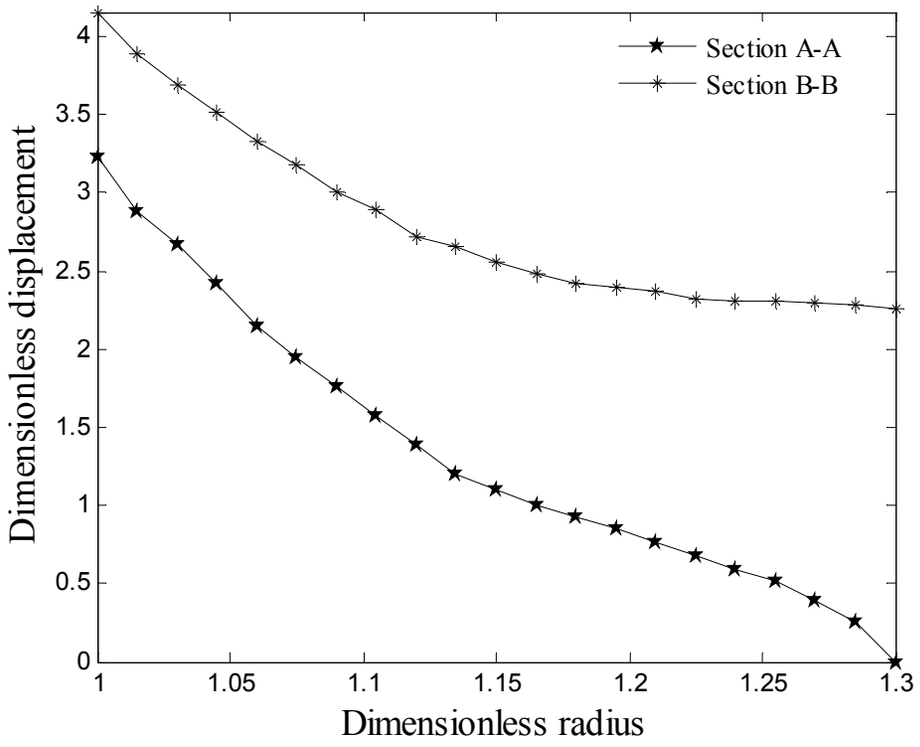


**Figure 14.** Total displacement distribution along the radius of asymmetric closed sphere.

### *5.3.2. Three- dimensional open sphere*

The geometry and loading condition as well as its boundary conditions are shown in Fig. 15. Three different boundary conditions are considered in this case. These boundary conditions are clamped-clamped, clamped-simply and simply-simply supported respectively.

The solution obtained by the software clearly indicates the most critical region of the sphere. In the most critical region normalized effective stress distribution and the total displacements are plotted in Figs. 16 and 17 along normalized radius at all node points for the above mentioned three boundary conditions. Fig 16 shows that in general the effective stresses are decreasing along radius to an absolute minimum and then increasing to their maximum values located at the outer surface of the vessel. For simply-simply supported boundary condition this absolute minimum is located near the outer surface of the vessel, however for the clamped-clamped condition it is nearly at the middle surface of the vessel. For the clamped-simply supported condition this minimum is somewhere between the previous two cases.

It has been found that the magnitude of effective stresses at all node points are higher for the clamped-clamped condition and are lower for the simply-simply supported condition. It can be observed from Fig. 17 that the maximum displacements for the three boundary conditions are located at the inner surface and they are decreasing to zero value at the outer surface of the sphere. It is also found that the displacement curve for simply-simply support condition is higher than other boundary conditions.

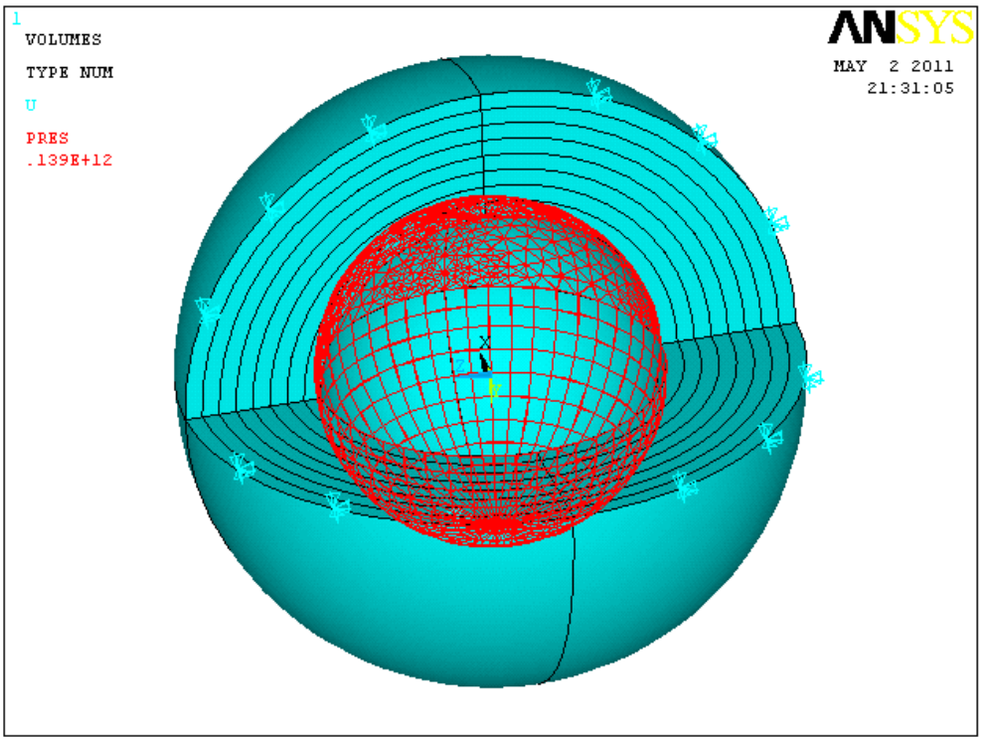


**Figure 15.** The three-dimensional finite element model for open sphere subjected to internal pressure with clamped-clamped boundary conditions.

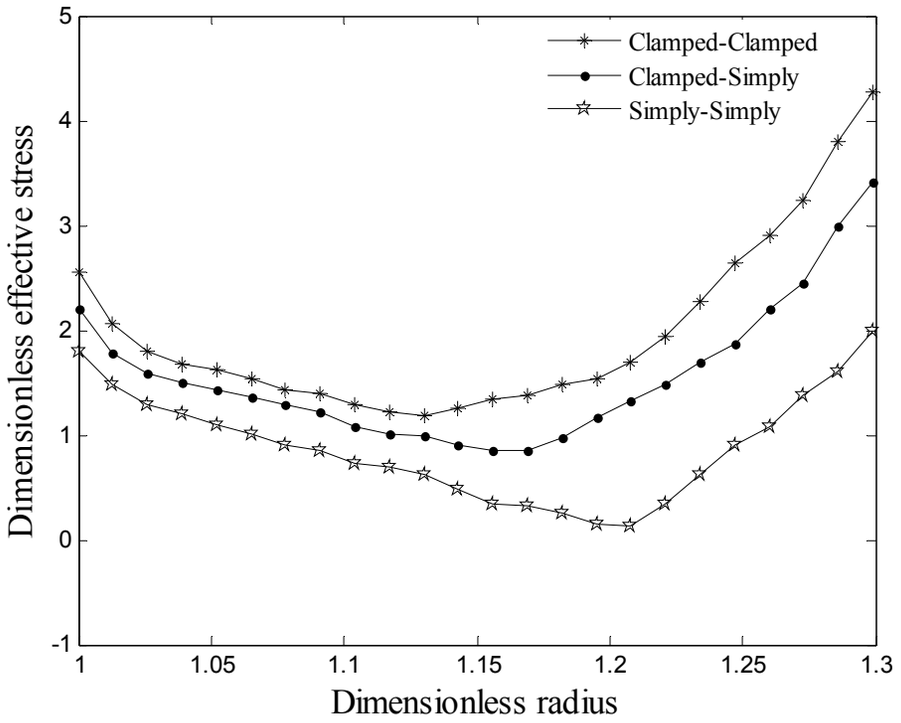


**Figure 16.** Effective stresses distribution along the radius of the open sphere with different boundary conditions.

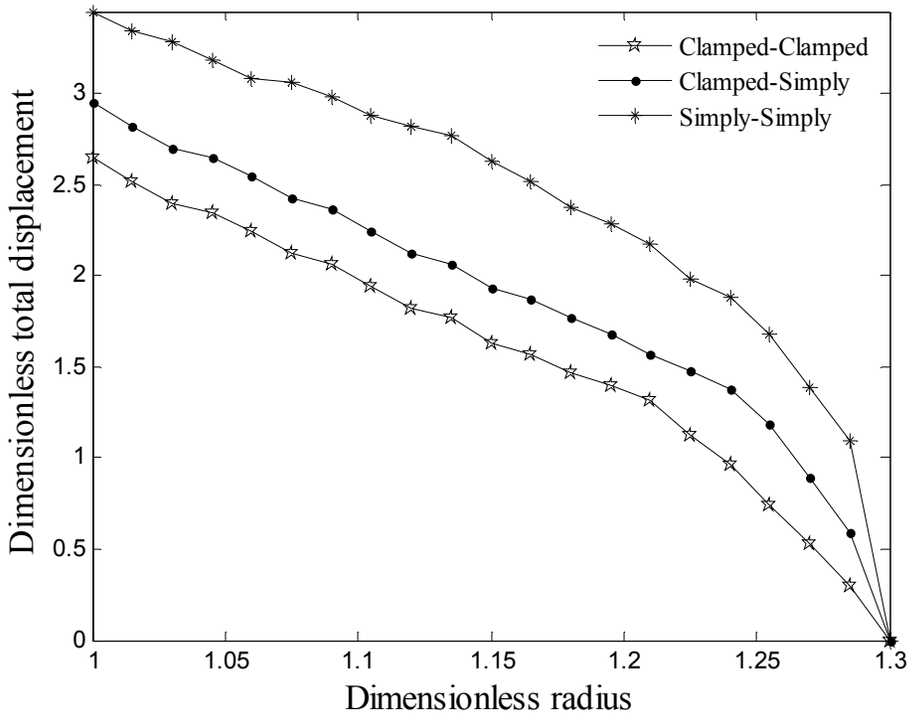


**Figure 17.** Total displacement distribution along the radius of the open sphere with different boundary conditions.

## 6. Conclusions

In this research, the electro-thermo-mechanical behavior of radially polarized FGPM hollow sphere was investigated. An analytic solution technique was developed for the electro-thermo-mechanical problem, where stresses were produced under combined thermomechanical and electrical loading conditions. Variation of normalized stresses, electric potential and displacement of four sets of boundary conditions for different material in-homogeneity parameters $\gamma$ were plotted against dimensionless radius. In general, radial stresses and electric potentials satisfy the mechanical and electrical boundary conditions at the inner and outer surfaces of the FGPM sphere. It was concluded that higher absolute values of compressive radial stresses are associated with the higher induced electric potentials throughout the thickness in all cases. It was found that the induced radial and circumferential stresses of an imposed electric potential is similar to the residual stresses locked in the sphere during the autofrettage process of these vessels. Therefore, one might concluded that by easily imposing an electric potential there is no need to autofrettage these vessels. It was interesting to see that the compressive circumferential stresses due to an external pressure were very similar to the induced circumferential stresses resulted from imposing an electric potential. Moreover a three-dimensional finite element analysis of an asymmetric sphere subjected to an internal pressure and a uniform temperature field has been carried out using ANSYS software. In this study closed and opened spheres with different boundary conditions were considered. The finite element analysis indicated that the values of effective stress and total displacement at all node points along the thickness of

the open sphere were the highest and lowest for the clamped-clamped condition, respectively.

## Appendix A

$$D_1=\frac{\gamma\left(C_1+E_1^2\right)+2C_1+2E_1^2}{C_1+E_1^2},D_2=\frac{\gamma\left(2C_2+2E_1E_2\right)+2C_2+2E_1E_2-2-2C_3-4E_2^2}{C_1+E_1^2},D_3=\frac{2E_2}{C_1+E_1^2}$$

$$D_4=\frac{\left(\gamma+1\right)\left(2C_2\alpha_\theta+C_1\alpha_r+E_1\left(2E_2\alpha_\theta+E_1\alpha_r\right)\right)+2\left(2C_2\alpha_\theta+C_1\alpha_r\right)+2\left(E_1-E_2\right)\left(2E_2\alpha_\theta+E_1\alpha_r\right)\left(\left(1+C_3\right)\alpha_\theta+C_2\alpha_r\right)}{\left(C_1+E_1^2\right)\left(\gamma+1\right)}$$

$$D_5=\frac{\gamma\left(4C_2\alpha_\theta-2C_1\alpha_r-2E_1\left(2E_2\alpha_\theta+E_1\alpha_r\right)\right)-2\left(2C_2\alpha_\theta+C_1\alpha_r\right)-\left(2E_1-E_2\right)\left(2E_2\alpha_\theta+E_1\alpha_r\right)+\left(2\left(1+C_3\right)\alpha_\theta+2C_2\alpha_r\right)}{\left(C_1+E_1^2\right)}$$

## Appendix B

$m_{ij}\ \ (i,j=1,...4)$ are the coefficient of $K_1$, $K_2$, $A_1$ and $A_2$ which defined as

$m_{11}=2C_2+C_1q_1+2E_1E_2+E_1^2q$, $m_{12}=2C_2+C_1q_2+2E_1E_2+E_1^2q_2$,

$$m_{13}=\frac{\left(2C_2+2E_1E_2+(1-\gamma)(E_1^2+C_1)\right)D_3}{(q_2+\gamma-1)(q_1+\gamma-1)}-2\left(E_1\right)$$

$m_{21}=\left(2C_2+C_1q_1+2E_1E_2+E_1^2q_1\right)\eta^{q_1-1+\gamma}$, $m_{22}=\left(2C_2+C_1q_2+2E_1E_2+E_1^2q_2\right)\eta^{q_2-1+\gamma}$,

$$m_{23}=\frac{\left(2C_2+2E_1E_2+(1-\gamma)(E_1^2+C_1)\right)D_3}{(q_2+\gamma-1)(q_1+\gamma-1)}-2\left(E_1\right)\eta^{-2},\ m_{31}=\left(\frac{2E_2}{q_1}+E_1\right),$$

$$m_{33}=\frac{\left(\gamma E_1-E_1-2E_2\right)D_3}{(q_2+\gamma-1)(q_1+\gamma-1)(1-\gamma)}+\frac{1}{(1+\gamma)},\ m_{41}=\left(\frac{2E_2}{q_1}+E_1\right)\eta^{q_1},\ m_{42}=\left(\frac{2E_2}{q_2}+E_1\right)\eta^{q_2}$$

$$m_{43}=\frac{\left(\gamma E_1-E_1-2E_2\right)D_3\,\eta^{1-\gamma}}{(q_2+\gamma-1)(q_1+\gamma-1)(1-\gamma)}+\frac{\eta^{-\gamma-1}}{(1+\gamma)},\ m_{41}=0,\ m_{24}=0,\ m_{34}=1,\ m_{44}=1$$

$b_i\ \ (i=1,2)$ are correspond to cases 1 and 24 which denoted as follows: $b_1=\sigma_r(1)$, $b_1=\sigma_r(\xi)$

## Author details

A. Ghorbanpour Arani, R. Kolahchi, A. A. Mosalaei Barzoki and A. Loghman
*Department of Mechanical Engineering, Faculty of Engineering, University of Kashan, Kashan, Iran*

F. Ebrahimi
*Department of Mechanical Engineering, Faculty of Engineering, International University of Imam Khomeini, Qazvin, Iran*

## 7. References


[1] P. Destuynder, A few remarks on the controllability of an aeroacoustic model using piezo-devices, Int. J. Holnicki-Szulc. (1999) 53–62.

[2] H.W. Jiang, F. Schmid, W. Brand, G.R. Tomlinson, Controlling pantograph dynamics using smart technology, Int. J. Holnicki-Szulc. (1999) 125–132.

[3] W.Q. Chen, Problems of radially polarized piezoelastic bodies, Int. J. solids struct. 36 (1998) 4317-4332.

[4] D.K. Sinha, Note on the radial deformation of a piezoelectric, polarized spherical shell with a symmetrical distribution, J. Acoust. Soc. 34 (1962) 1073–1075.

[5] A. Ghorbanpour, S. Golabi, M. Saadatfar, Stress and electric potential fields in piezoelectric smart spheres, J. Mech. Sci. Tech. 20 (2006) 1920–1933.

[6] M. Saadatfar, A. Rastgoo, Stress in piezoelectric hollow sphere under thermal environment, J. Mech. Sci. Tech, 22 (2008) 1460–1467.

[7] H.L. Dai, X. Wang, Thermo-electro-elastic transient response, Int. J. solids struct. 42 (2005) 1151–1171.

[8] H.L. Dai, Y.M. Fu, Electromagnetotransient stress and perturbation of magnetic field vector in transversely isotropic piezoelectric solid sphere, Mater. Sci. Eng. B 129 (2006) 86–92.

[9] L.H. You, J.J. Zhang, X.Y. You, Elastic analysis of internally pressurized thick-walled spherical pressure vessels of functionally graded materials, Int. J. Press. Vess. Pip. 82 (2005) 347–354.

[10] H.J. Ding, H.M. Wang, W.Q. Chen, Analytical solution for a non-homogeneous isotropic piezoelectric hollow sphere, Arch. Appl. Mech. 73 (2003) 49–62.

[11] A. Ghorbanpour Arani, R. Kolahchi, A.A. Mosallaie Barzoki, Effect of material in-homogeneity on electro-thermo-mechanical behaviors of functionally graded piezoelectric rotating cylinder, J. Appl. Math. Model. 35 (2011) 2771–2789.

[12] H.M. Wang, Z.X. Xu, Effect of material inhomogeneity on electromechanical behaviors of functionally graded piezoelectric spherical structures, Comput. Mater. Sci. 48 (2010) 440–445.

[13] A. Ghorbanpour, M. Salari, H. Khademizadeh, A. Arefmanesh, Magnetothermoelastic problems of FGM spheres, Arch. Appl. Mech. (2010) 189-200.

[14] V. Sladek, J. Sladek, Ch. Zhang, Transient heat conduction analysis in functionally graded materials by the meshless local boundary integral equation method, Comput. Mater. Sci. 28 (2003) 494-504.

[15] J. Sladek, V. Sladek, P. Solek, A. Saez, Dynamic 3D axisymmetric problems in continuously non-homogeneous piezoelectric solids, Int. J. solids struct. 45 (2008) 4523–4542.

[16] Institute of Electrical and Electronics Engineers. Standard on Piezoelectricity, Std (1978) 176-1978 IEEE, New York.

[17] Y.C. Fungn, Foundations of Solid Mechanics, Prentice-Hall, New York, 1965.

[18] H.F. Tiersten, Linear Piezoelectric Plate Vibrations, Plenum Press, New York, 1969

[19] A. Manonukul, F.P.E. Dunne, D. Knowles, S. Williams, Multiaxial creep and cyclic plasticity in nickel-base superalloy C263, Int. J. Plasticity, 21 (2005) 1–20.
[20] H. Martin, ELASTICITY Theory, Applications and Numerics, Elsevier Inc, London, 2005.
[21] H.J. Ding, W.Q. Chen, Three Dimensional Problems of Piezoelasticity, Nova Science, New York, 2001.
[22] M. Sadeghian, H. Ekhteraei Toussi, Axisymmetric yielding of functionally graded spherical vessel under thermo-mechanical loading, Comput. Mater. Sci. 50 (2011) 975–981.
[23] A. Salehi-Khojin, N. Jalili, A comprehensive model for load transfer in nanotube reinforced piezoelectric polymeric composites subjected to electro-thermo-mechanical loadings. Compos: Part B. 39 (2008) 986–998.
[24] Zh. Li, Ch. Wang, Ch. Chen, Effective electromechanical properties of transversely isotropic piezoelectric ceramics with microvoids, Comput. Mater. Sci. 27 (2003) 381–392.
[25] N. Jalili, Piezoelectric-Based Vibration Control from Macro to Micro/Nano Scale Systems, Boston, 2010.
[26] M.H. Babaei, Z.T. Chen, Analytical solution for the electromechanical behavior of a rotating functionally graded piezoelectric hollow shaft, Arch. Appl. Mech. 78 (2008) 489–500.
[27] H.L., Dai, L. Hong, Y. M., Fu, X. Xiao, Analytical solution for electro-magneto-thermo-elastic behaviors of a functionally graded piezoelectric hollow cylinder, J. Appl. Math. Model. 34 (2010) 343–357.
[28] M. Saadatfar, A.S. Razavi, Piezoelectric hollow cylinder with thermal gradient, J. Mech. Sci. Tech. 23 (2009) 45–53.